frontiers | Frontiers in Earth Science

TYPE Original Research
PUBLISHED 17 January 2023
DOI 10.3389/feart.2022.1026310

OPEN ACCESS

EDITED BY
Shenghua Cui,
Chengdu University of Technology, China

REVIEWED BY
Xiangbo Bu,
Universitat Politecnica de Catalunya, Spain
Yang Lu,
Hohai University, China

*CORRESPONDENCE
Shan Dong,
dongshan@cug.edu.cn

SPECIALTY SECTION
This article was submitted to Geohazards and Georisks, a section of the journal Frontiers in Earth Science

RECEIVED 23 August 2022
ACCEPTED 14 November 2022
PUBLISHED 17 January 2023

CITATION
Peng Y, Dong S, Lu Z, Zhang H and Hou W (2023), A method for calculating permanent displacement of seismic-induced bedding rock landslide considering the deterioration of the structural plane.
Front. Earth Sci. 10:1026310.
doi: 10.3389/feart.2022.1026310

A method for calculating permanent displacement of seismic-induced bedding rock landslide considering the deterioration of the structural plane

Yulin Peng[1,2], Shan Dong[1,2]*, Zhichun Lu[3], Heng Zhang[1,2] and Weihua Hou[1,2]

[1]Badong National Observation and Research Station of Geohazards, China University of Geosciences, Wuhan, China, [2]Three Gorges Research Center for Geohazards, China University of Geosciences, Wuha, China, [3]Changjiang Institute of Survey, Planning, Design and Research Corporation, Wuhan, China

The mechanism of seismic-induced bedding rock landslide is distinct from that of slope instability/landslide in normal gravity conditions; their failure modes are mainly characterized by vibration deterioration effect of rock mass structural plane due to a seismic loading, which has a significant effect on the stability of the bedding rock landslide. Several advanced methods have been proposed to assess earthquake-induced bedding rock landslide. However, the quantitative evaluation of the vibration deterioration effect of structural plane, along with its application in the dynamic stability analysis of bedding rock slopes, remains a challenging topic that requires further study. In this study, on the basic of the analysis of the cyclic shear condition and the cyclic shear test of the structural plane, the expressions to calculate the dilatancy angle and basic friction angle of structural plane under cyclic shear loading are studied. A deterioration formula for structural plane shear strength is proposed, which fully considers the deterioration effect during cyclic shear. Furthermore, a new calculating method of the seismic-induced permanent displacement of the bedding rock landslide, which introduces the deterioration effect of the structural plane, is developed. A case study was used to compare the permanent displacement calculated with the proposed method with those obtained using the Newmark and Qi methods, which demonstrates the effectiveness and applicability of the proposed method.

KEYWORDS

structural plane, deterioration effect, seismic-induced bedding rock landslide, dynamic analysis model, permanent displacement

1 Introduction

When the magnitude of an earthquake exceeds Ms 4.0, landslides can be induced in sensitive areas; when the magnitude of an earthquake exceeds Ms 6.0, many landslides can be induced simultaneously (Keefer 1984; Rodríguez et al., 1999; Keefer 2000). Larger earthquakes can induce thousands of landslides over a wide area. For example, the Wenchuan Ms 8.0 earthquake in China triggered nearly 200,000 landslides, making it the largest, densest, widest, and most catastrophic seismic-induced landslide events caused by a single earthquake ever recorded. Bedding rock landslide is a common type of rock landslide, and is controlled by the interlayer structural planes of the rock mass. When subjected to an earthquake or dynamic loads, such slopes are prone to the occurance of overall bedding slip. In recent years, earthquakes have induced many bedding rock landslides, such as the Daguangbao and Tangjiashan landslides caused by the 2008 Wenchuan earthquake (Ms 8.0) in China (Burchfiel et al., 2008; Hu et al., 2009; Huang and Li, 2009; Cui et al., 2021), and the Arato-sawa landslide caused by the 2008 Iwate-Miyagi Naoriku earthquake (Ms 7.0) in Japan (Moriya et al., 2010; Ryoichi et al., 2010; Setiawan et al., 2016). These seismic-induced landslides lead to serious losses of life and property. Therefore, the study of seismic-induced bedding rock landslide is of great and practical significance.

When the seismic loading is strong, the cyclic shear phenomenon occurs along the interlayer structural plane and the slipping body consequently moves along the structural plane. As demonstrated in Figure 1, taking the horizontal seismic acceleration as an example, when the upward component of the horizontal seismic force along the interlayer structural plane ($M\ddot{u}_g \cos\beta$) is greater than the resulatant force of the shear strength of the interlayer structural plane and the weight component of the sliding body ($Mg \sin\beta$), a cyclic shear mode of the slipping body will occur. During this process, the initial morphological characteristics of the interlayer structural planes are destroyed in terms of the shearing or wearing of the undulations, resulting in the deterioration of the shear strength of the interlayer structural plane which directly influences the stability of the slope. Extensive studies have been conducted on the cyclic shear strength of the structural plane (Souley et al., 1995; Homand et al., 2001; Jafari et al., 2003; Premadasa et al., 2012; Mirzaghorbanali et al., 2014; Zheng et al., 2015; Li et al., 2021a; 2021b; Zhou et al., 2021; Li, 2022a; 2022b), and it was found that, when rock mass is sheared along a structural plane, undulations and the friction of the contact sections of the structural plane have a direct effect on the shearing resistance. Under the earthquake action, the seismic loading causes vibration deterioration of the shear characteristics of the structural plane. This is mainly shown in the following aspects: 1) the peak shear strength of the structural plane decreases with the increase of relative shear velocity; 2) under the cyclic shear (from seismic loading), the undulant angle α_k decreases; and 3) under the seismic loading, the frictional coefficient of the structural plane decreases gradually. In addition, previous studies (Tulinov and Molokov, 1971; Papaliangas et al., 1990; Indraratna et al., 1999; Indraratna et al., 2005; Mroz and Giambanco, 2015; Dong et al., 2020) have demonstrated that under a seismic cyclic shear loading, structural plane undulations are sheared and worn gradually, and a large amount of debris is generated and filled in the inside of the contact sections, which directly affects the frictional characteristics of the structural plane. Therefore, the degradation effect of the frictional characteristics of the structural plane must be considered when performing the stability calculation of bedding rock landslide under a seismic cyclic shear loading.

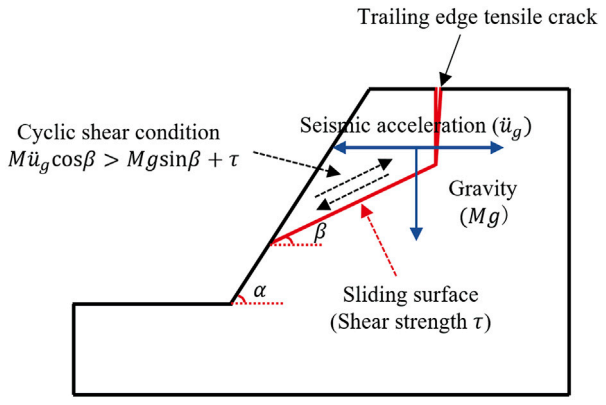

FIGURE 1
Condition of cyclic shear under horizontal seismic acceleration.

Wang and Zhang (1982) found that the movement rate and cumulative displacement of rock blocks have a direct deterioration effect on the dynamic frictional coefficient, and initially tried to incorporate the degradation effect of the structural plane into the calculation method of the sliding displacement of rock slopes. Crawford and Curran (1981, 1982) also proposed a method of calculating the seismic permanent displacement of rock slope introducing the deterioration effect of cumulative displacement and motion velocity on structural plane. Based on the work by Wang and Zhang (1982) and Crawford and Curran (1981, 1982), Qi (2007) proposed a seismic permanent displacement calculation method of planar sliding and wedge sliding problem considering the effect of shear rate and cumulative relative displacement on the deterioration of structural surface roughness. Through the experimental analysis of direct shear experiment and shaking table test, Bakun-Mazor et al. (2012) found that, under the strong ground motion, the dynamic analysis of rock slopes should consider the effect of shear velocity on the friction force of the structural plane. By integrating the influencing factors of

vibration wear and relative velocity, Ni et al. (2013) presented mathematical expressions for the vibration degradation effect of a structural face through experimental research, and applied them to the calculation of the dynamic stability analysis of rock slopes using numerical simulation method. Liu et al. (2016) found that the shear strength of structural plane was reduced due to the wear of wave angle and relative velocity between rock blocks during the process of earthquake action, and a mathematical model to calculate the deterioration of the structural plane and a numerical calculation procedure were established. Based on the Newmark and residual thrust methods, Cen (2017) proposed a theoretical model and dynamic analysis with time-history, considering the entire shear process deterioration effect of bedding rock landslide. Dong et al. (2020) proposed deterioration formulas for structural plane shear strength parameters under cyclic shear loading, and on the basis of the cyclic structural plane shear test, they proposed a calculation method for rock landslide displacement by introducing the deterioration effect of the structural plane. However, existing researches on bedding rock landslide stability calculation introducing the effect of structural plane degradation have not yet yielded a definitive and well-recognized method, and the analysis of the dynamic stability of bedding rock landslide with consideration of structural plane vibration degradation required in-depth study.

In conclusion, the effect of seismic loading on the stability of bedding rock landslide lies in the influence of seismic loading on inertial force and the deterioration effect of seismic loading on shear strength (frictional coefficient) of interlayer structural plane. The present study, firstly, investigated the shear-strength deterioration effect of a structural plane. Then, based on the simplified dynamic calculation model of the bedding-rock landslide and introducing the vibration-induced deterioration effect of the structural plane, a new calculating method of the seismic-induced permanent displacement of the bedding rock landslide is further developed. And the motivation of this study is to further improve the understanding of seismic-induced landslide mechanisms by means of a relatively systematic investigation into the dynamic characteristics, instability mechanisms, and stability evaluation methods of bedding-rock landslides under seismic loading.

2 Deterioration of the structural plane under the cyclic shear

2.1 Cyclic shear test on structural plane

It is difficult to obtain and sample natural structural planes with complex surface undulations, and the consistency related to the sampling cannot be guaranteed. However, it has been proved that it is feasible to use rock structure samples prepared from cement mortar and other similar materials to replace the surface

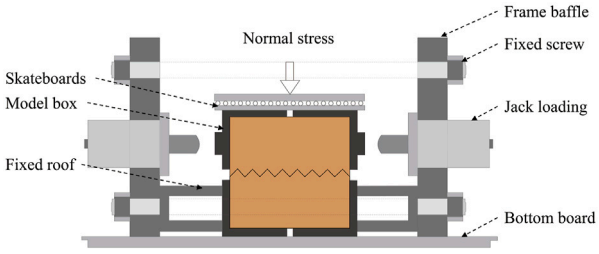

FIGURE 2
Schematic view of RJDT-A shear box.

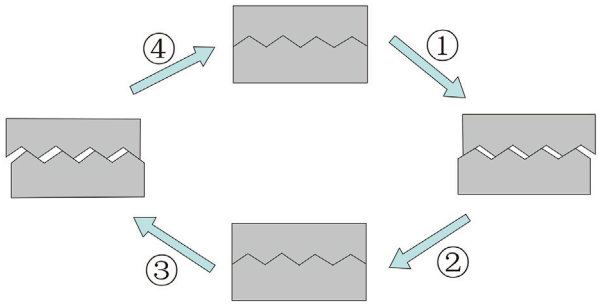

FIGURE 3
A single cyclic shear process of the rock mass structural plane.

morphology and undulation of natural structural planes (Einstein et al., 1983; Plesha, 1987; Yang et al., 2001; Jafari et al., 2003; Li et al., 2008; Du et al., 2011). When using simulated structural planes to replace natural structural planes for direct shear tests, the wear degree and failure mode of simulated structural planes are similar to those of natural structural planes. The existing research results (Ladanyi and Archambault 1970; Yang et al., 2001; Jafari et al., 2003; Shen and Zhang, 2010) show that although there are differences between the sawtooth structural plane and the natural structural plane, the shear test with sawtooth structural plane is usually reasonable and can catch the surface morphology and undulations of the structural plane. Using cement mortar as the similar material, Liu et al. (2011) prepared sawtooth structural plane specimens with different initial undulant angles of 16°, 25°, 33°, 40°and 45°, respectively. Using an RJDT-A shear testing device (Figure 2), Liu et al. (2011) carried out cyclic shear tests on structural planes under four kinds normal stresses of 0.8, 1.6, 2.4, and 3.2 MPa, respectively. Due to the limitations of the RJDT-A shear testing device, the relative maximum shearing displacement was set to be ±10 mm, and the cyclic number was set to be 10 repetitions. In the shear process, the lower shear box remains stationary, and the specimen is sheared by the

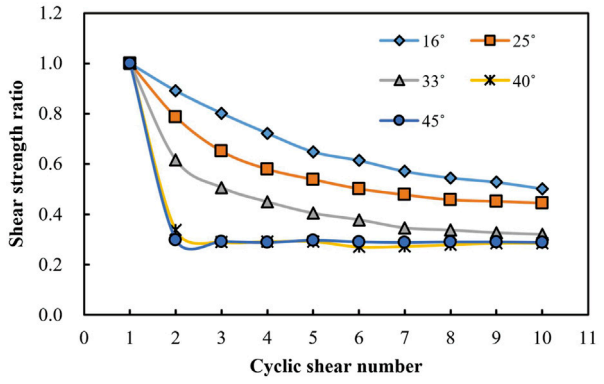

FIGURE 4
Variation of shear strength ratio (D_n) of structural planes with five kinds of initial undulant angles with cyclic shear number under σ_n =0.8 MPa (Liu et al., 2011).

horizontal motion of the upper shear box. A single cyclic shear process of the rock mass structural plane is illustrated in Figure 3.

2.2 Shear strength deterioration effect

Introducing the shear strength ratio D_n of the structural plane as the shear strength deterioration index, Liu et al. (2011) obtained the variation law of shear strength of structural plane. The peak shear strength of the nth cyclic shear is expressed as τ_n, then the D_n is defined as:

$$D_n = \frac{\tau_n}{\tau_1}. \tag{1}$$

The shear strength ratio D_n ($0.0 \le D_n \le 1.0$) reflects the shear strength degradation after several shear cycles: the closer D_n is to 1, the lesser the influence of strength deterioration induced by cyclic shear is. On the contrary, the closer D_n is to 0, the greater the influence of strength deterioration induced by cyclic shear is.

Figure 4 demonstrates the variation of shear strength ratios D_n of structural planes with five kinds of initial undulant angles with cyclic shear number under σ_n = 0.8 MPa. It is found that the peak shear strength of structural plane specimens with five kinds of initial undulant angles decreases with the increase cyclic shear number, though the decreasing trend is different. The D_n with an initial undulant angle of 16° decreases at the lowest rate with the increase of cyclic shear number and keeps a steady decreasing trend, while the D_n with an initial undulant angle of 45° decreases at the highest rate with the increase of cyclic shear number and remains basically unchanged after the 2-th cyclic shear. And the decreasing speed of D_n increases with the increase of initial undulant angle. On the whole, the higher the undulations of the structural plane are, the lower the shear resisting force of the undulations is, and the occurrence of more significant shearing or wearing damage in the cycle shear is more likely. Thus, for a specimen with higher undulant angles, the shearing or wearing damage of the surface undulations is mainly in the early stage of cyclic shear, and the degree of shearing or wearing damage changes insignificantly in the subsequent cyclic shear, and for a specimen with smaller undulant angle, the undulations on the surface has strong shear resisting force, the shearing or wearing damage is mainly caused by multiple shear or cumulative wear. Thus, the D_n of the specimens with smaller undulant angle decrease more slowly with the increase of the cyclic shear number.

2.3 Shear strength of structural plane introducing the relative shear velocity effect

When the shear movement of rock mass occurs, the shear resisting force mainly consists of the undulations of the structural plane and the friction of the contact sections:

$$\varphi = \varphi_b + \alpha_k \tag{2}$$

where φ denotes the friction angle of the structural plane, φ_b denotes the basic friction angle, and α_k denotes the undulant angle.

On the basis of many direct shear tests on the rough structural plane, Barton and Choubey (1977) proposed to replace the undulant angle with the dilatancy angle:

$$\alpha_d = \frac{JRC}{2} \lg \frac{JCS}{\sigma_n} \tag{3}$$

where α_d denotes the dilatancy angle, JRC denotes the roughness coefficient, JCS denotes the uniaxial compressive strength of the intact rock, and σ_n denotes the normal stress.

Furthermore, Barton (1973) further proposed the following shear strength equation for structural plane:

$$\tau = \sigma_n \tan\left(JRC \cdot \lg \frac{JCS}{\sigma_n} + \varphi_b \right) \tag{4}$$

where τ denotes the peak shear strength of structural plane.

Then, Eqs. 3, 4 can be combined as follows:

$$\tau = \sigma_n \tan\left(2\alpha_d + \varphi_b\right) \tag{5}$$

And after nth cyclic shear, the friction angle of the structural plane can be obtained:

$$\varphi = 2\alpha_n + \varphi_n \tag{6}$$

where n denotes the cyclic shear number, α_n and φ_n denote the average dilatancy angle and the basic friction angle after the nth cyclic shear, respectively.

So, after nth cyclic shear, the peak shear strength of structural plane can be obtained:

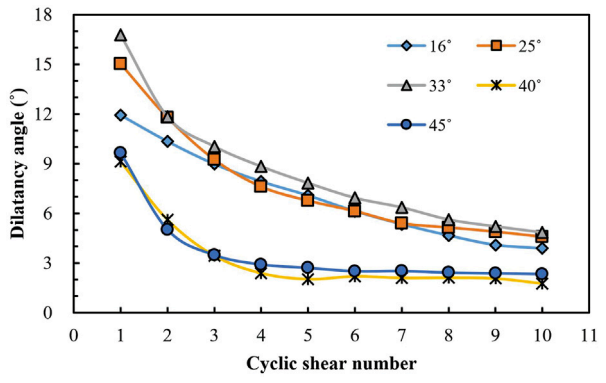

FIGURE 5
Variation of the average dilatancy angle with cyclic shear number with five kinds of initial undulant angles (Liu et al., 2013a).

$$\tau = \sigma_n \tan\left(2\alpha_n + \varphi_n\right) \tag{7}$$

According to the strength characteristic test of structural plane under different shear velocity, Li et al. (2006) concluded that the peak shear strength of structural plane decreases with the increase of relative shear velocity. Thus, an exponential decay functional relationship exists between the peak strength and the relative shear velocity. According to the research of Wang and Zhang (1982) and Li et al. (2006), Liu (2017) further proposed to express the relative velocity coefficient as follows:

$$\gamma(t) = \gamma_r + (1 - \gamma_r)e^{-a|\dot{x}(t)|} \tag{8}$$

where $\dot{x}(t)$ denotes the relative shear velocity of the structural plane (m/s), γ_r denotes the convergence value of the relative shear velocity correlation coefficient, and a denotes the undetermined factor. Referring to the research of Ni et al. (2013), $\gamma_r = 0.9$, $a = 25$.

Therefore, combining Eqs. 7, 8, the shear strength of the structural plane introducing the relative shear velocity effect can be obtained as follows:

$$\tau = \gamma(t) \cdot \sigma_n \tan\left(2\alpha_n + \varphi_n\right) \tag{9}$$

2.4 Dilatancy angle and basic friction angle during cyclic shear

According to Eq. 9, the key to determining the shear strength of a structural plane during the cyclic shear is to derive variation laws of the dilatancy angle and the basic friction angle. Therefore, this section will focus on the analysis of the variation laws of the dilatancy angle and the basic friction angle during the cyclic shear.

2.4.1 Dilatancy angle of the structural plane

Figure 5 demonstrates the variation of the average dilatancy angle with cyclic shear number for the cases of different initial undulant angles (Liu et al., 2013a). It can be found that with the increase of initial undulant angle, the dilatancy angle at the first cyclic shear of the structural plane increases firstly and then decreases (16°<25°<33°,16°>40°>45°). This is mainly due to the difference of shear failure modes between structural planes with high undulant angle and those with medium undulant angle, and the initial undulant angles of the 40° and 45° structural planes are more serious. On the whole, for structural planes with different initial undulant angles, the dilatancy angle gradually decrease, first rapidly, then more gradually and incline be stable slowly with the increase of cyclic shear number.

On the basis of above experimental results, Liu et al. (2013b) further found that there exists a negative exponential distribution relationship between the average dilatancy angle of the structural plane and the cyclic shear number, and the following expression is proposed:

$$\alpha_n = \alpha_0\left(Ae^{-n/B} + C\right) \tag{10}$$

where α_0 denotes initial undulant angle of the structural plane. It is worth noting that when $\sigma_n = 0$ or the shear is not performed, $\alpha_n = \alpha_0$.

The wear coefficient R_s of the average shear dilatancy angle can be further expressed as:

$$R_s = \frac{\alpha_n}{\alpha_0} = Ae^{-n/B} + C. \tag{11}$$

When $n = 0$, $R_s = 1$, and $A + C = 1$, Eq. 11 can be adapted as:

$$R_s = Ae^{-n/B} + C = A\left(e^{-n/B} - 1\right) + 1 \tag{12}$$

Therefore,

$$\alpha_n = \alpha_0 R_s = \alpha_0\left[A\left(e^{-n/B} - 1\right) + 1\right] \tag{13}$$

Based on Liu et al. (2013b) study, under the same uniaxial compressive strength of the intact rock σ_c, there exists a linear relationship between the parameter A or B and normal stress σ_n. Thus, the equations of A and B can be assumed as follows:

$$A = a\sigma_n + b \tag{14}$$

$$B = c\sigma_n + d \tag{15}$$

where parameters a, b, c, and d denote constants that are linked to uniaxial compressive strength of the intact rock σ_c. The relationships between a, b, c, and d and the uniaxial compressive strength of the intact rock σ_c can be determined by regression analysis.

2.4.2 Basic frictional angle of the structural plane

Based on Dong et al. (2020), the average shear dilatancy angle of the structural plane can reflect the degradation of undulations during the cyclic shearing, and the basic frictional angle and the

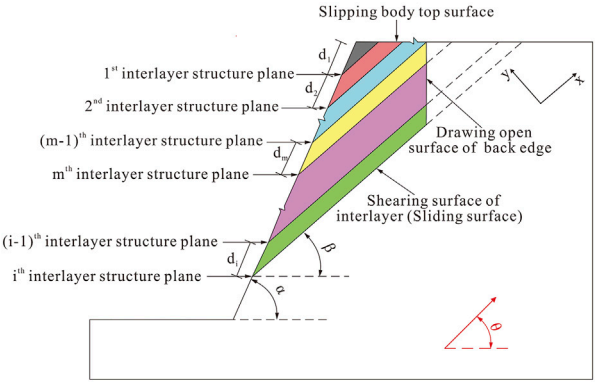

FIGURE 6
Generalized diagram of dynamic model of bedding rock slope.

average shear dilatancy angle have the same variation trend. Thus, the following equation exists:

$$\frac{\alpha_0 - \alpha_n}{\alpha_0 - \alpha_r} = \frac{\varphi_0 - \varphi_n}{\varphi_0 - \varphi_r}. \tag{16}$$

where α_0 and φ_0 are the initial undulant angle and initial basic friction angle of the structural plane, respectively; α_r and φ_r are the residual dilatancy angle and residual basic friction angle, respectively.

According to Eq. 16, the basic frictional angle of the structural plane after the nth cyclic shear can be obtained:

$$\varphi_n = \frac{\alpha_n(\varphi_0 - \varphi_r) - \varphi_0\alpha_r + \varphi_r\alpha_0}{\alpha_0 - \alpha_r}. \tag{17}$$

where φ_0 can be converted by the inclination experiment of the smooth structural plane.

The residual equivalent frictional angle (φ_s^*) can be defined as follows:

$$\varphi_s^* = \arctan\left(\tau_r/\sigma_n\right) \tag{18}$$

where τ_r is the residual shear stress, φ_s^* is the residual equivalent frictional angle. Since the equivalent friction angle (φ_s^*) is mainly composed of residual basic friction angle (φ_r) and the residual dilatancy angle (α_r), and the residual basic frictional angle (φ_r) can be obtained:

$$\varphi_r = \varphi_s^* - \alpha_r = \arctan\left(\tau_r/\sigma_n\right) - \alpha_r \tag{19}$$

Thus, according to Eqs. 17, 19, the expression of basic friction angle φ_n can be expressed as:

$$\varphi_n = \frac{(\alpha_0 - \alpha_n)\left[\arctan\left(\tau_r/\sigma_n\right) - \alpha_r\right] + (\alpha_n - \alpha_r)\varphi_0}{\alpha_0 - \alpha_r}. \tag{20}$$

3 Calculation method for permanent displacement

3.1 Dynamic analysis model

A simplified dynamic calculation model of a bedding rock slope is illustrated in Figure 6, assuming that the potential sliding body produces unstable sliding along the rock stratum of the ith layer, di denotes the exposed length of ith rock stratum, α denotes the slope gradient, β denotes the dip angle of the rock stratum, $\ddot{u}_g$ denotes the seismic acceleration, and θ denotes the angle between the direction of seismic acceleration and the horizontal direction.

It should be noted that the quadrilateral area is composed of slope surface, sliding surface, slipping body top surface, and tensile crack surface of back edge of the rock slope. And the area of potential sliding body is determined by:

$$S_i = \frac{1}{2}\left(\sum_{n=1}^{i} d_n\right)^2 \frac{\sin\alpha\sin(\alpha-\beta)}{\sin\beta} - \frac{1}{2}\left(\sum_{n=m}^{i} d_n\right)^2 \frac{\tan\beta sin^{\,2}(\alpha-\beta)}{sin^{\,2}\beta}. \tag{21}$$

The gravity of the potential sliding body in layer i is G_i,

$$G_i = \gamma_i(S_i - S_{i-1}) \tag{22}$$

where γ_i is the volumetric weigh of the ith rock stratum. And the total gravity of the sliding body G_{it} is:

$$G_{it} = \sum_{n=1}^{i} G_n \tag{23}$$

According to the force equilibrium analysis in dynamic analysis model, in the Y direction

$$N = G_{it}\cos\beta + \frac{G_{it}}{g}\ddot{u}_g\sin(\theta-\beta) \tag{24}$$

and in the X direction

$$T = G_{it}\sin\beta + \frac{G_{it}}{g}\ddot{u}_g\cos(\theta-\beta) \tag{25}$$

where T denotes the parallel (shear) reaction forces, N denotes the orthogonal (normal) reaction forces, g denotes the acceleration owing to gravity. The seismic loading can act as both driving force and resisting force. Thus, Eqs. 24, 25 are vector equations, and the $\ddot{u}_g$ changes with its symbol: when the seismic loading acts as the driving force, the symbol of $\ddot{u}_g$ is positive, and when the seismic loading acts as the resisting force, the symbol of $\ddot{u}_g$ is negative.

3.2 Critical acceleration

For the bedding rock landslide, the influence of cohesion (c) is mainly focused on the first cyclic shear process. Once the sliding mass generates cyclic shear under strong ground motion,

the influence of cohesion (c) on shear strength is commonly ignored (Dong et al., 2020). The critical acceleration a_c can be defined as the minimum seismic acceleration that leads to the potential sliding body to overcome available shear resistance and to move. If $\ddot{u}_g > a_c$, the potential sliding body will overcome the available shear resistance and obtain sliding displacement. According to Eqs. 9, 25, the safety factor (F_s) of sliding body can be expressed as:

$$F_s = \frac{\text{available shear resistance}}{\text{driving force}} = \frac{\tau}{T} = \frac{\gamma(t)\cdot\sigma_n \tan(2\alpha_n + \varphi_n)}{G_{it}\sin\beta + \frac{G_{it}}{g}\ddot{u}_g \cos(\theta - \beta)}. \quad (26)$$

The safety factor $F_s = 1$ is the critical condition for landslide instability, so assuming $F_S = 1$, the critical seismic acceleration is expressed as follows:

$$a_c = \frac{g[\gamma(t)\tan(2\alpha_n + \varphi_n)\cos\beta - \sin\beta]}{\cos(\theta - \beta) - \gamma(t)\sin(\theta - \beta)\tan(2\alpha_n + \varphi_n)}. \quad (27)$$

3.3 Vibration balance equation

Based on Figure 6, the X-direction vibration balance equation can be expressed as follows:

$$M\ddot{u}_g\cos(\theta - \beta) + Mg\sin\beta - \gamma(t)N\tan(2\alpha_n + \varphi_n) = M\ddot{s} \quad (28)$$

where M is the mass of the potential sliding body, and

$$M = \frac{G_{it}}{g}. \quad (29)$$

And according to Eqs. 24, 28, 29 the acceleration of the potential sliding body can be expressed as follows:

$$\begin{aligned}\ddot{s} &= \ddot{u}_g\cos(\theta - \beta) + g\sin\beta \\ &\quad - \{\gamma(t)[g\cos\beta + \ddot{u}_g\sin(\theta - \beta)]\tan(2\alpha_n + \varphi_n)\} \\ &= \ddot{u}_g[\cos(\theta - \beta) - \gamma(t)\sin(\theta - \beta)\tan(2\alpha_n + \varphi_n)] \\ &\quad - g[\gamma(t)\cos\beta\tan(2\alpha_n + \varphi_n) - \sin\beta] \end{aligned} \quad (30)$$

3.4 Calculation procedure of permanent displacement

After obtaining the dilatancy angle and basic friction angle after nth cyclic shear, the calculation procedures of permanent displacement are as follows:

1) The seismic acceleration $\ddot{u}_g$ is divided into $n\Delta t$ with time-history, and the critical acceleration a_c can be obtained based on Eq. (27)
2) When the seismic acceleration $\ddot{u}_g > a_c$, sliding displacement of the slope may be produced under seismic acceleration. The original acceleration of the sliding body $(\ddot{s})_0$ can be acquired based on Eq. 30.
3) The occurrence of sliding depends on whether $(\dot{s})_1$ is greater than zero. If $(\dot{s})_1 > 0$, the time-history displacement $(s)_{m1}$ can be integrated; if $(\dot{s})_1 < 0$, the next time-history can be integrated until m_1-th time-history, where $(\dot{s})_{m1} \geq 0$.
4) Repeating the step (3) until the nth time-history, and finally obtaining the permanent displacement $(s)_n = (s)_{n-1} + (\dot{s})_n\Delta t$.

4 Case study

It is very difficult to find the monitoring data of sliding displacement of bedding rock slope under seismic loading. Thus, in order to illustrate the effectiveness and applicability of the proposed calculating method for permanent displacement, referring to the experimental research results of Liu et al. (2013b), a calculation case study was conducted. In the case study, the main parameters are as follows: the normal stress was 1.6 MPa, the basic friction angle was 30.5°, the initial undulant angle was 16°, the uniaxial compressive strength of the intact rock was 30 MPa, the residual shear strength was 0.798 MPa, the residual dilatancy angle was 7.744°, and the cyclic shear number n=10.

Based on dynamic analysis model in Figure 6, assuming that the slope gradient was 30°, the dip angle of rock stratum was 15°, the weight of rock mass was 23 kN/m^3, the thickness of each layer of the rock stratum was equal, the length of the exposed surface of each layer was 10 m. Under the seismic loading, the average relative shear velocity $\dot{x}(t)$ of interlayer structural plane is 8 mm/s, and according to Eq. 8, the relative velocity coefficient γ (t) was approximately 0.98. And the landslide slided from the fifth interlayer structural plane. The horizontal acceleration ($\theta = 0$) is used as the seismic acceleration in Figure 7.

4.1 Calculation of dilatancy angle and basic friction angle

Based on the experimental results of wear coefficient of the average dilatancy angle (R_s) for specimens with the initial undulant angle of 16° (Table 1), by fitting the experimental results as Eqs. 14, 15, the correlation parameters A and B were obtained with Eq. 11, and Figures 8A,B demonstrate the fitting relationship between correlation parameters A and B and the normal stress σ_n with different uniaxial compressive strengths of the intact rock σ_c. Then, the fitting relationship between correlation parameters a, b, c, and d and the uniaxial compressive strength of the intact rock σ_c were obtained by regression analysis, and the results are demonstrated in Figures

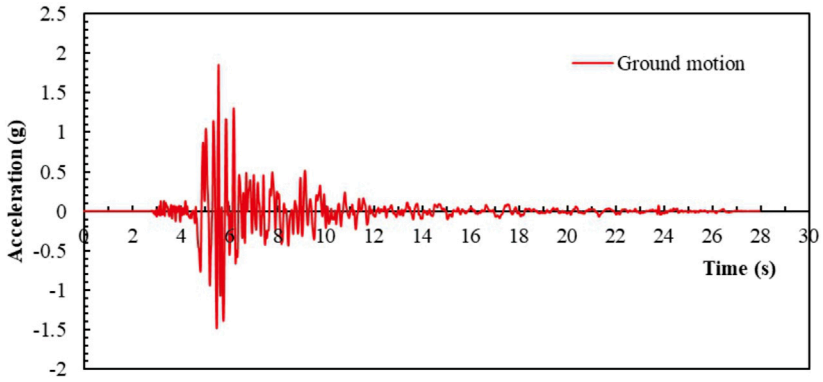

FIGURE 7
Seismic acceleration used in the case study.

8C,D, with the expressions of A and B being obtained, as indicated below:

$$A = (0.0039\sigma_n - 0.0263)\sigma_c - 0.0233\sigma_n + 1.2222 \quad (31)$$

$$B = (0.0839 - 0.0074\sigma_n)\sigma_c - 0.3031\sigma_n + 1.3562 \quad (32)$$

Based on Eqs. 31, 32, after 10-th shear cycles, the values of parameters A and B were 0.583 and 3.033, respectively. According to Eqs. 13, 20, the variations of the dilatancy angle and basic friction angle with the increase of cyclic shear number were obtained (Figure 9). The dilatancy angle and basic friction angle gradually decreased and tended to be stable with the increase of the cyclic shear number. After 10-th cyclic shear, the calculated final dilatancy angle was 7.015°. From Eq. 20, the basic friction angle after 10-th cyclic shear was 17.728°.

4.2 Calculation of permanent displacement

After obtaining the dilatancy angle and basic friction angle, based on the analysis steps of permanent displacement, the variations of critical acceleration and permanent displacement with the cyclic shear number are obtained respectively (Figure 10), where the number of cycle shear is 0, indicating that the deterioration effect of the structural plane is not considered. With the increase of the cyclic shear number, the critical acceleration decreases gradually, especially when cyclic shear number is greater than 5, the critical acceleration decreases slowly and tends to be stable. The permanent displacement increases gradually with the increase of cyclic shear number. And the permanent displacement of the slope is obtained to be 0.015 m when the deterioration effect is not considered. Before the 5-th cyclic shear, the permanent displacement increases linearly with the cyclic shear number, and then the permanent displacement increases slowly and gradually tends to be stable, and the calculated final permanent displacement is 0.420 m after 10-th cyclic shear.

4.3 Comparison with other methods

4.3.1 Newmark method

Newmark (1965) introduced seismic loading into rock slope stability analyses and further proposed Newmark sliding rigid block method. For the Newmark method, the critical acceleration is:

$$k_y = \tan(\varphi - \beta) \quad (33)$$

$$a_c = k_y g \quad (34)$$

where k_y denotes the yield coefficient, φ denotes the frictional angle between the sliding body and the sliding surface, and β denotes the dip angle of the rock stratum. For the Newmark method, the permanent displacement is determined by the double integral of the part where the seismic acceleration is greater than the critical acceleration a_c.

4.3.2 Qi method

Based on the vibration degradation law of the undulant angle by using the research results of Plesha (1987), Qi (2007) proposed a permanent displacement calculation method of rock slope, in which the variation of undulant angle is:

$$\alpha_k = (\alpha_k)_0 \exp\left(-cW^P\right) \quad (35)$$

where $(\alpha_k)_0$ denotes the initial undulant angle, W^P denotes the plastic work, and c denotes the structural plane damage coefficient (m^2/J). Hutson and Dowding (1990) experimentally verified the accuracy of Eq. 35 and proposed the empirical expression of the damage coefficient c:

TABLE 1 Experimental results of R_s of specimens with the initial undulant angle of 16° (Liu et al., 2013b).

Specimen number	σ_c = 10 MPa				σ_c = 20 MPa				σ_c = 30 MPa			
	J01	J06	J11	J16	J21	J26	J31	J36	J41	J46	J51	J56
σ_n *n*th	0.8 MPa	1.6 MPa	2.4 MPa	3.2 MPa	0.8 MPa	1.6 MPa	2.4 MPa	3.2 MPa	0.8 MPa	1.6 MPa	2.4 MPa	3.2 MPa
0	1.00	1.00	1.00	1.00	1.00	1.00	1.00	1.00	1.00	1.00	1.00	1.00
1	0.651	0.577	0.516	0.404	0.739	0.650	0.602	0.577	0.901	0.880	0.818	0.716
2	0.398	0.288	0.224	0.141	0.643	0.479	0.383	0.310	0.776	0.739	0.654	0.555
3	0.245	0.175	0.140	0.075	0.560	0.386	0.276	0.200	0.703	0.656	0.566	0.478
4	0.163	0.118	0.101	0.053	0.494	0.325	0.212	0.146	0.657	0.611	0.514	0.425
5	0.123	0.081	0.069	0.043	0.440	0.272	0.174	0.106	0.620	0.573	0.469	0.384
6	0.099	0.065	0.051	0.030	0.378	0.231	0.142	0.079	0.592	0.541	0.441	0.353
7	0.085	0.055	0.038	0.026	0.331	0.199	0.121	0.063	0.573	0.525	0.417	0.329
8	0.075	0.053	0.036	0.021	0.283	0.170	0.107	0.056	0.556	0.504	0.393	0.312
9	0.068	0.049	0.032	0.019	0.253	0.162	0.091	0.061	0.544	0.494	0.382	0.297
10	0.069	0.046	0.031	0.019	0.236	0.160	0.080	0.059	0.535	0.484	0.369	0.283

10.3389/feart.2022.1026310

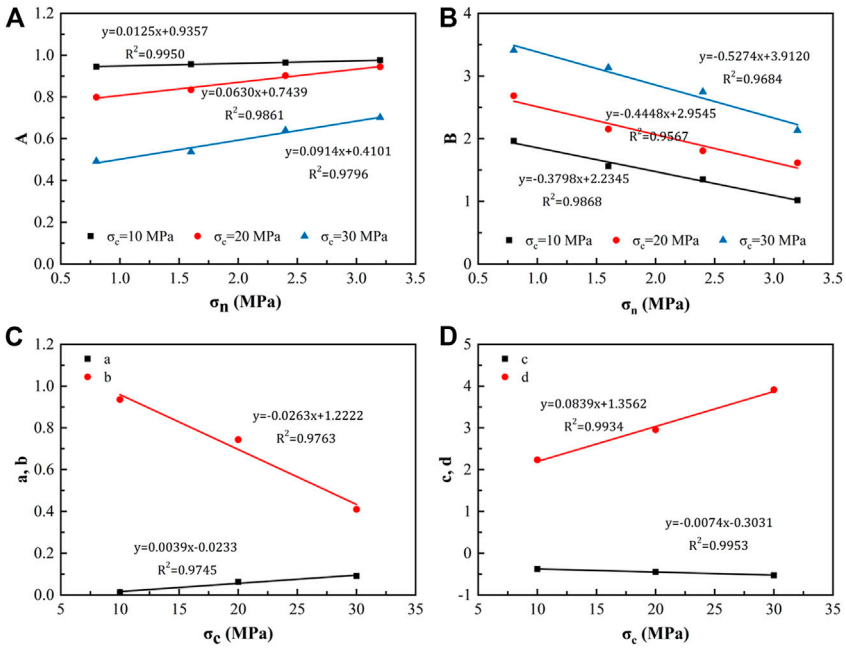

FIGURE 8
Fitting relationships of main parameters. **(A)** Fitting relationships between A and σ_n; **(B)** Fitting relationships between B and σ_n; **(C)** Fitting relationships between a, b and σ_c; **(D)** Fitting relationships between c, d and σ_c.

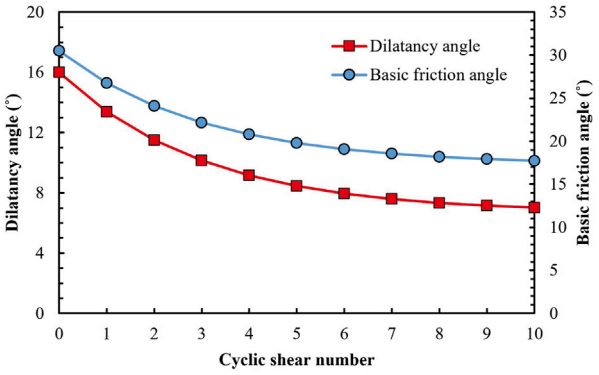

FIGURE 9
Variations of dilatancy angle and basic friction angle with cyclic shear number.

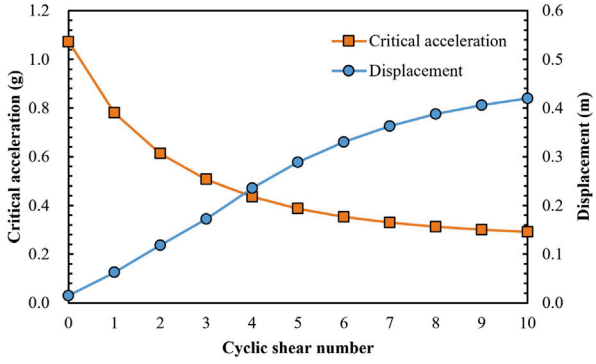

FIGURE 10
Variations of critical acceleration and permanent displacement with the cyclic shear number.

$$c = -0.114JRC\left(\frac{\sigma_n}{\sigma_c}\right) \tag{36}$$

In the Qi method, the basic friction angle φ_b is:

$$\tan\varphi_b = \frac{\cos(\theta-\beta)a_c + \sin\beta\cos\beta}{\cos\beta + \sin(\theta-\beta)a_c}. \tag{37}$$

The initial critical acceleration $a_c(0,0)$ is expressed as:

$$a_c(0,0) = -\frac{\sin(\beta-\varphi)}{\cos(\theta-\beta+\varphi)}. \tag{38}$$

Considering the cumulative displacement and relative velocity effect, the expression of critical acceleration with displacement is proposed as follows:

$$a_c = Pa_c(0,0) \tag{39}$$

where P is the reduction coefficient, between 0 and 1.

TABLE 2 Calculation results using different methods.

Methods	Calculation results	
	Critical acceleration/g	Displacement/m
Newmark method	0.613	0.095
Proposed Method	0.291	0.420
$P = 1$	0.613	0.107
$P = 0.6$ 5	0.398	0.266
Qi method$P = 0.5$	0.306	0.393
$P = 0.4$	0.245	0.507

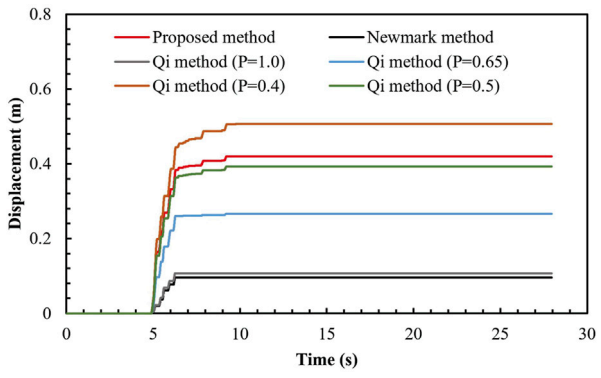

FIGURE 11
Permanent displacements obtained by different methods.

And the acceleration of the sliding body is expressed as:

$$\ddot{x} = \frac{g\cos(\theta - \beta + \varphi)}{\cos\varphi}\left(\ddot{u}_g - a_c\right). \tag{40}$$

The seismic acceleration $\ddot{u}_g$ is divided into $n\Delta t$ with time-history. The occurrence of sliding depends on whether the velocity of the sliding body $(\dot{x})_1$ is greater than zero. If $(\dot{x})_1 > 0$, the time-history displacement $(x)_{m1}$ can be integrated; if $(\dot{x})_1 < 0$, the next time-history can be integrated until $m1$-th time-history, where $(\dot{x})_{m1} \geq 0$. Then, repeating the above steps until the nth time-history, and finally obtaining the permanent displacement $(x)_n = (x)_{n-1} + (\dot{x})_n \Delta t$.

4.4 Comparison

The comparative calculation results of critical acceleration are presented in Table 2. The critical acceleration of the Newmark method is 0.613 g. For the Qi method, when $P = 1$, the critical acceleration obtained is the same as that obtained with the Newmark method, and it can be found that the critical acceleration of the Qi method reduces with a decreasing of reduction coefficient P. This is because the shear strength gradually deteriorates during the cyclic shear process, and the ground motion load required to initiate a landslide is reduced. In the proposed method, the critical acceleration is smaller than that obtained with the Newmark method, and is between those of the Qi method with $p = 0.4$ and $p = 0.5$. It is worth noting that, the critical acceleration obtained with the Newmark method remains constant under seismic loading, while the critical acceleration reduces gradually with the deterioration of the structural plane in the proposed method and the Qi method, which is more in line with actual observations.

The calculation results of permanent displacement are shown in Table 2; Figure 11. In the proposed method, the cumulative displacement curve obtained is between those of the Qi method with $p = 0.4$ and $p = 0.5$, and in contrast the cumulative displacement is closer to the Qi method with $p = 0.5$. However, the permanent displacement obtained by Qi method and the proposed method is larger than that provided by the Newmark method, which illustrates that the deterioration effect of the structural plane has a significant effect on the calculation of permanent displacement, and the calculation methods that considers the deterioration effect are more conservative and reliable in terms of evaluating the stability of seismic-induced landslides.

5 Conclusion

In this study, based on the analysis of the cyclic shear condition under seismic loading, a new method for calculating the permanent displacement of the bedding-rock landslide was proposed by introducing the degradation effect of structural plane, and the following main conclusions can be obtained:

1) When the upward component of the horizontal seismic force along the interlayer structural plane is greater than the resulatant force of the shear strength of the interlayer structural plane and the weight component of the sliding body, a cyclic shear mode of the slipping body will occur.
2) Under the cyclic shear loading, the deterioration of the structural plane mainly consists of the relative shear velocity effect, dilatancy angle degradation and basic frictional angle degradation.
3) To verify the effectiveness and applicability of the proposed calculating method for permanent displacement, using a case study, the calculated displacement results using the proposed method were compared with those obtained using the Newmark and Qi method. It was found that under seismic loading, the degradation effect of the structural plane has a direct effect on the permanent displacement and stability of the bedding rock landslide. The calculation method proposed in this paper potentially serves as reference for engineering design, calculation, and application.

Data availability statement

The original contributions presented in the study are included in the article/Supplementary Material, further inquiries can be directed to the corresponding author.

Author contributions

YP and SD were responsible for the main manuscript writing and idea discussions; Other authors were responsible for the prepare the paper language, figures, and tables. All authors have reviewed and agreed to the published version of the manuscript.

Funding

The Fellowship of China Postdoctoral Science Foundation (Grant No. 2022M712949); the Open Fund Project of Badong National Observation and Research Station of Geohazards, China University of Geosciences (Grant No. BNORSG202210); the State Key Laboratory of Geohazard Prevention and Geoenvironment Protection of the Chengdu University of Technology Open Fund (Grant No. SKLGP 2019K010); the State Key Laboratory of Geohazard Prevention and Geoenvironment Protection of the Chengdu University of Technology Open Fund (Grant No. SKLGP 2020K015).

Conflict of interest

Author ZL was employed by the company Changjiang Institute of Survey, Planning, Design and Research Corporation.

The remaining authors declare that the research was conducted in the absence of any commercial or financial relationships that could be construed as a potential conflict of interest.

Publisher's note

References

Bakun-Mazor, D., Hatzor, Y. H., and Glaser, S. D. (2012). Dynamic sliding of tetrahedral wedge: The role of interface friction. *Int. J. Numer. Anal. Meth. Geomech.* 36 (3), 327–343. doi:10.1002/nag.1009

Barton, N. R., and Choubey, V. (1977). The shear strength of rock joints in theory and practice. *Rock Mech.* 10 (1-2), 1–54. doi:10.1007/bf01261801

Barton, N. R. (1973). Review of a new shear strength criterion for rock joints. *Eng. Geol.* 7 (4), 287–332. doi:10.1016/0013-7952(73)90013-6

Burchfiel, B. C., Royden, L. H., Hilst, R. D. V. D., Hager, B. H., Chen, Z., King, R. W., et al. (2008). A geological and geophysical context for the wenchuan earthquake of 12 may 2008, sichuan, people's Republic of China. *Gsa Today* 18 (7), 4–11. doi:10.1130/gsatg18a.1

Cen, D. (2017). *Tensional rupture and low-friction initiation mechanism of bedding landslides triggered by mega-earthquakes*. Chongqing: Chongqing University.

Crawford, A. M., and Curran, J. H. (1982). The influence of rate- and displacement-dependent shear resistance on the response of rock slopes to seismic loads. *Int. J. Rock Mech. Min. Sci. Geomechanics Abstr.* 19 (1), 1–8. doi:10.1016/0148-9062(82)90704-5

Crawford, A. M., and Curran, J. H. (1981). The influence of shear velocity on the frictional resistance of rock discontinuities. *Int. J. Rock Mech. Min. Sci. Geomechanics Abstr.* 18 (6), 505–515. doi:10.1016/0148-9062(81)90514-3

Cui, S., Pei, X., Jiang, Y., Wang, G., Fan, X., Yang, Q., et al. (2021). Liquefaction within a bedding fault: Understanding the initiation and movement of the Daguangbao landslide triggered by the 2008 Wenchuan Earthquake (Ms = 8.0). *Eng. Geol.* 295, 106455. doi:10.1016/j.enggeo.2021.106455

Dong, S., Feng, W., Yin, Y., Hu, R., and Zhang, G. (2020). Calculating the permanent displacement of a rock slope based on the shear characteristics of a structural plane under cyclic loading. *Rock Mech. Rock Eng.* 53 (53), 4583–4598. doi:10.1007/s00603-020-02188-y

Du, S., Hu, Y., Hu, X., and Guo, X. (2011). Comparison between empirical estimation by JRC-JCS model and direct shear test for joint shear strength. *J. Earth Sci.* 22 (3), 411–420. doi:10.1007/s12583-011-0193-6

Einstein, H. H., Veneziano, D., Baecher, G. B., and O'Reilly, K. J. (1983). The effect of discontinuity persistence on rock slope stability. *Int. J. Rock Mech. Min. Sci. Geomechanics Abstr.* 20 (5), 227–236. doi:10.1016/0148-9062(83)90003-7

Homand, F., Belem, T., and Souley, M. (2001). Friction and degradation of rock joint surfaces under shear loads. *Int. J. Numer. Anal. Meth. Geomech.* 25 (10), 973–999. doi:10.1002/nag.163

Hu, X., Huang, R., Shi, Y., Lu, X., and Wang, X. (2009). Analysis of blocking river mechanism of Tangjiashan landslide and dam-breaking mode of its barrier dam. *Chin. J. Rock Mech. Eng.* 28 (1), 181–189.

Huang, R., and Li, W. (2009). Development and distribution of geohazards triggered by the 5.12 Wenchuan Earthquake in China. *Sci. China Ser. E-Technol. Sci.* 52 (4), 810–819. doi:10.1007/s11431-009-0117-1

Hutson, R. W., and Dowding, C. H. (1990). Joint asperity degradation during cyclic shear. *Int. J. Rock Mech. Min. Sci. Geomechanics Abstr.* 27 (2), 109–119. doi:10.1016/0148-9062(90)94859-r

Indraratna, B., Welideniya, H. S., and Broen, E. T. (2005). A shear strength model for idealised infilled joints under constant normal stiffness (CNS). *Geotech* 55 (3), 215–226.

Indraratna, B., Haque, A., and Aziz, N. (1999). Shear behaviour of idealized infilled joints under constant normal stiffness. *Geotechnique* 49 (3), 331–355. doi:10.1680/geot.1999.49.3.331

Jafari, M. K., Hosseini, K. A., Pellet, F., Boulon, M., and Buzzi, O. (2003). Evaluation of shear strength of rock joints subjected to cyclic loading. *Soil Dyn. Earthq. Eng.* 23 (7), 619–630. doi:10.1016/s0267-7261(03)00063-0

Keefer, D. K. (1984). Landslides caused by earthquakes. *Geol. Soc. Am. Bull.* 95, 406–421. doi:10.1130/0016-7606(1984)95<406:lcbe>2.0.co;2

Keefer, D. K. (2000). Statistical analysis of an earthquake-induced landslide distribution the 1989 Loma Prieta, California event. *Eng. Geol.* 58 (3-4), 231–249. doi:10.1016/s0013-7952(00)00037-5

Ladanyi, B., and Archambault, G. (1970). "Simulation of shear behavior of a jointed rock mass," in *Proc.11th syrup. On rock mechanics: Theory and practice* (New York: AIME), 105–125.

Li, B., Jiang, Y., Koyama, T., Jing, L., and Tanabashi, Y. (2008). Experimental study of the hydro-mechanical behavior of rock joints using a parallel-plate model containing contact areas and artificial fractures. *Int. J. Rock Mech. Min. Sci. (1997).* 45 (3), 362–375. doi:10.1016/j.ijrmms.2007.06.004

Li, H., Deng, J., Feng, P., Pu, C., Arachchige, D., and Cheng, Q. (2021a). Short-term nacelle orientation forecasting using bilinear transformation and ICEEMDAN framework. *Front. Energy Res.* 9, 780928. doi:10.3389/fenrg.2021.780928

Li, H., Deng, J., Yuan, S., Feng, P., and Arachchige, D. (2021b). Monitoring and identifying wind turbine generator bearing faults using deep belief network and EWMA control charts. *Front. Energy Res.* 9, 799039. doi:10.3389/fenrg.2021.799039

Li, H., Feng, H., and Liu, B. (2006). Study on strength behaviors of rock joint under different shearing deformation velocities. *Rock Soil Mech.* 25 (12), 2435–2440.

Li, H. (2022a). SCADA data based wind power interval prediction using LUBE-based deep residual networks. *Front. Energy Res.* 10, 920837. doi:10.3389/fenrg.2022.920837

Li, H. (2022b). Short-term wind power prediction via spatial temporal analysis and deep residual networks. *Front. Energy Res.* 10, 920407. doi:10.3389/fenrg.2022.920407

Liu, B., Li, H., and Liu, Y. (2013a). Experimental study of deformation behavior of rock jointsunder cyclic shear loading. *Rock Soil Mech.* 34 (09), 2475–2488.

Liu, B., Li, H., Liu, Y., and Xia, X. (2013b). Generalized damage model for asperity and shear strength calculation of joints under cycle shear loading. *Chin. J. Rock Mech. Eng.* 32 (2), 3000–3008. doi:10.3969/j.issn.1000-6915.2013.z2.003

Liu, B., Li, H., and Zhu, X. (2011). Experimental simulation study of strength deterioration of rock joints under cyclic shear loading. *Chin. J. Rock Mech. Eng.* 30 (10), 2033–2039.

Liu, X., Liu, Y., He, C., and Li, W. (2016). Dynamic stability analysis of the bedding rock slope considering the vibration deterioration effect of the structural plane. *Bull. Eng. Geol. Environ.* 77, 87–103. doi:10.1007/s10064-016-0945-8

Liu, Y. (2017). *Study on cumulative damage evolution mechanism and stability of bedding rock slope in reservoir area under frequent microseismic*. Chongqing: Chongqing University.

Mirzaghorbanali, A., Nemcik, J., and Aziz, N. (2014). Effects of shear rate on cyclic loading shear behaviour of rock joints under constant normal stiffness conditions. *Rock Mech. Rock Eng.* 47 (5), 1931–1938. doi:10.1007/s00603-013-0453-0

Moriya, H., Abe, S., Ogita, S., and Higaki, D. (2010). Structure of the large-scale landslide at the upstream area of Aratozawa Dam induced by the Iwate-Miyagi Nairiku earthquake in 2008. *J. Jpn. Landslide Soc.* 47 (2), 77–83. doi:10.3313/jls.47.77

Mroz, Z., and Giambanco, G. (2015). An interface model for analysis of deformation behaviour of discontinuities. *Int. J. Numer. Anal. Methods Geomech.* 20 (1), 1–33. doi:10.1002/(sici)1096-9853(199601)20:1<1::aid-nag799>3.0.co;2-l

Newmark, N. M. (1965). Effects of earthquakes on dams and embankments. *Geotechnique* 15 (2), 139–160. doi:10.1680/geot.1965.15.2.139

Ni, W., Tang, H., Liu, X., and Wu, Y. (2013). Dynamic stability analysis of rock slope considering vibration deterioration of structural planes under seismic loading. *Chin. J. Rock Mech. Eng.* 32 (3), 492–500. doi:10.3969/j.issn.1000-6915.2013.03.008

Papaliangas, T., Lumsden, A. C., Hencher, S. R., and Manolopoulou, S. (1990). Shear strength of modelled filled rock joints. *Proc International Symposium on Rock Joints, Loen*, 275–283. doi:10.1016/0148-9062(91)92234-p

Plesha, M. E. (1987). Constitutive models for rock discontinuities with dilatancy and surface degradation. *Int. J. Numer. Anal. Methods Geomech.* 11 (4), 345–362. doi:10.1002/nag.1610110404

Premadasa, W., Indraratna, B., Mizargobanali, A., and Oliveira, D. (2012). "Shear behaviour of rock joints under cyclic loading," in *Australia-New Zealand conference on geomechanics: Ground engineering in A changing world.*

Qi, S. (2007). Evaluation of the permanent displacement of rock mass slope considering deterioration of slide surface during earthquake. *Chin. J. Geotech. Eng.* 29 (3), 452–457. doi:10.3321/j.issn:1000-4548.2007.03.024

Rodríguez, C. E., Bommer, J. J., and Chandler, R. J. (1999). Earthquake-induced landslides: 1980-1997. *Soil Dyn. Earthq. Eng.* 18 (5), 325–346. doi:10.1016/s0267-7261(99)00012-3

Ryoichi, Ohno., Shin-ichi, Yamashina., Takanari, Y. A. M. A. S. A. K. I., Tomofumi, K. O. Y. A. M. A., Fumitoshi, E. S. A. K. A., and Shikoh, K. A. S. A. I. (2010). Mechanisms of a large-scale landslide triggered by the earthquake in 2008: A study of arato-sawa landslide. *J. Jpn. Landslide Soc.* 47 (2), 84–90. doi:10.3313/jls.47.84

Setiawan, H., Sassa, K., Takara, K., Miyagi, T., and Fukuoka, H. (2016). Initial pore pressure ratio in the earthquake triggered large-scale landslide near aratozawa dam in miyagi prefecture, Japan. *Procedia Earth Planet. Sci.* 16, 61–70. doi:10.1016/j.proeps.2016.10.007

Shen, M., and Zhang, Q. (2010). Experimental study of shear deformation characteristics of rock mass discontinuities. *Chin. J. Rock Mech. Eng.* 29 (4), 713–719.

Souley, M., Homand, F., and Amadei, B. (1995). An extension to the Saeb and Amadei constitutive model for rock joints to include cyclic loading paths. *Int. J. Rock Mech. Min. Sci. Geomechanics Abstr.* 32 (2), 101–109. doi:10.1016/0148-9062(94)00039-6

Tulinov, R., and Molokov, L. (1971). "Role of joint filling material in shear strength of rocks," in *Symposium of international society of rock mechanics* (Nancy.

Wang, S., and Zhang, J. (1982). Dynamic analysis of sliding stability of slope rock mass. *Chin. J. Geol.* 2, 162–170.

Yang, Z., Di, C., and Yen, K. (2001). The effect of asperity order on the roughness of rock joints. *Int. J. Rock Mech. Min. Sci. (1997).* 38 (5), 745–752. doi:10.1016/s1365-1609(01)00032-6

Zheng, B., Qi, S., Zhan, Z., Zou, Y., and Zhang, S. (2015). Effect of shear rate on the strength characteristics of rock joints. *J. Earth Sci. Envir.* 37 (5), 101–110.

Zhou, J., Wei, J., Yang, T., Zhang, P., Liu, F., and Chen, J. (2021). Seepage channel development in the crown pillar: Insights from induced microseismicity. *Int. J. Rock Mech. Min. Sci. (1997).* 145, 104851. doi:10.1016/j.ijrmms.2021.104851